Low Sidelobe Super-Resolution Lens Based on Fermat Spiral-Arranged Dielectric Nano-Columns

Jiali Liao, Jinrong Lan, Yanling Sun, Wei Li, Lin Ma, and Zhenzhong Lu

***Abstract*— Super-resolution lenses (SRLs) based on the principle of optical super-oscillation are composed of subwavelength structural units, which can achieve precise control of light properties through suitable design. A bio-inspired SRL structure with Fermat Spiral-arranged dielectric nano-column is proposed in this letter for the first time. Owing to the unequally spaced arrangement of the Fermat Spiral, the proposed SRL can effectively suppress the sidelobe of the focal field and achieve a high focusing efficiency. The focusing properties of the SRL are investigated detailedly by simulation. The focusing efficiency and the peak sidelobe ratio of the focal field are 72.8% and 16.02 dB, respectively, at the wavelength of 1.55 μm. And an ultra-wide working bandwidth of 200 nm are achieved by the proposed SRL with high focusing efficiencies and low sidelobe energies in the whole bandwidth. In addition, the sub-diffraction limit focusing is achieved by only controlling the radius of the nano-columns, and the bio-inspired Fermat Spiral-arranged SRL exhibits a large tolerance of the fabrication error.**

***Index Terms*— Fermat spiral, SRL, low-sidelobe energy, sub-diffraction limit focusing.**

I. Introduction

SUPER-RESOLUTION lenses (SRLs), as an important application of metasurfaces, have been extensively studied in recent years [1], [2], [3]. The SRLs are composed of subwavelength units, and each unit cell plays a role as a control unit [4]. SRLs break the dependence on the thickness of optical materials, which can not only realize the miniaturization and integration of optical systems, but also realize ultra-diffractive focusing [5], [6].

In recent years, many kinds of SRLs have been reported, such as a SRL with an enlarged field of view and depth of focus, titanium dioxide (TiO_2) based multiwavelength achromatic SRL and switchable polarization-multiplexed SRL for achromatic sub-diffraction focusing [7], [8], [9]. However, achromatic SRLs usually have evident sidelobes of the focal point, and the sidelobes not only weaken the properties of the focal field, but also lead to the focal point accounting for a very small part of the incident energy. An angularly polarized SRL with a NA of 0.96 was reported to achieve a maximum sidelobe ratio of 36.7%, and an amplitude and phase-controllable SRL was reported to suppress the sidelobe with the sidelobe level of −16.3 dB [10], [11], but these SRLs could only suppress the sidelobe at a single working wavelength. These non-ignored sidelobes of SRLs are the important obstacles to a series of applications, thus it is necessary to suppress the sidelobe of the focal field in a wide working wavelength range [12], [13].

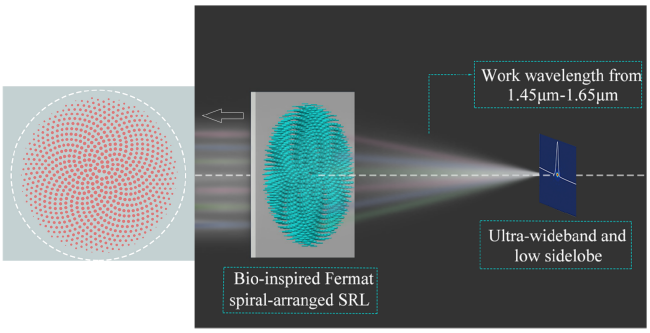

Fig. 1. Schematic diagram of the bio-inspired Fermat Spiral-arranged dielectric nano-column SRL.

In this letter, for the first time, a super-resolution lens based on bio-inspired Fermat Spiral-arranged nano-dielectric-columns is proposed, as shown in Fig.1. Benefiting from the bio-inspired structure and complementary metal–oxide–semiconductor (CMOS) compatible Si units, the sub-diffraction-limited focusing is conveniently achieved by controlling the radii of the nano-columns at different positions. The focusing properties of the proposed bio-inspired SRL are investigated. Within the wide working wavelength band from 1450 nm to 1650 nm, the focal spot sizes are from $0.47\frac{\lambda}{NA}$ to $0.488\frac{\lambda}{NA}$, which are evidently smaller than the Abbe diffraction limit of $0.51\frac{\lambda}{NA}$. The focusing efficiencies of the proposed SRL is higher than 67.5% in the working wavelength range, with the highest value of 72.8% at 1550 nm. Particularly, the peak sidelobe ratios (PSLR) maintain higher than 15.29 dB in the whole working band, with the highest

Manuscript received 26 May 2023; revised 16 September 2023; accepted 15 October 2023. Date of publication 20 October 2023; date of current version 27 October 2023. This work was supported in part by the National Natural Science Foundation of China under Grant 62005207 and Grant 61701505; in part by the 2021 Open Project Fund of Science and Technology on Electromechanical Dynamic Control Laboratory, China; in part by the Open Research Fund of the State Key Laboratory of Pulsed Power Laser Technology under Grant SKL 2019 KF 06; and in part by the Natural Science Foundation of Shaanxi Province, China, under Grant 2019JQ-648 and Grant 2022JM-341. *(Corresponding authors: Jiali Liao; Yanling Sun.)*

Jiali Liao is with the School of Optoelectronic Engineering, Xidian University, Xi'an 710071, China, and also with the Science and Technology on Electromechanical Dynamic Control Laboratory, Xi'an 710065, China (e-mail: liaojiali@xidian.edu.cn).

Jinrong Lan, Yanling Sun, Wei Li, Lin Ma, and Zhenzhong Lu are with the School of Optoelectronic Engineering, Xidian University, Xi'an 710071, China.

Color versions of one or more figures in this letter are available at https://doi.org/10.1109/LPT.2023.3326311.

Digital Object Identifier 10.1109/LPT.2023.3326311

value of 16.02 dB at 1550 nm. In addition, the bio-inspired Fermat Spiral-arranged SRL exhibits a large fabrication error tolerance. The SRL can achieve achromatic sub-diffraction focusing with low sidelobe, providing a new approach to realize microscopic imaging.

II. Design of the Fermat Spiral-Arranged SRL

The unit cells of the SRL in this letter are polarization-insensitive structures with perfect rotational symmetry, and the phase control is realized just by changing the geometric size of the unit cells. Therefore, the SRL is mainly designed by the control of the transmission phase. When the equivalent refractive index of the medium is n_{eff}, and a light wave with a wavelength of λ travels a distance h in the medium, the transmission phase shift is expressed as:

$$\varphi = \frac{2\pi}{\lambda} n_{eff} h \tag{1}$$

where $2\pi/\lambda$ represents the wave vector in free space, and h represents the thickness or height of the medium. It can be seen from the formula that the transmission phase is determined by the equivalent refractive index and the thickness of the medium. The transmission phase type of dielectric SRLs is based on the equivalent refractive index theory. The duty cycle of the unit cells is changed to realize the regulation of the equivalent refractive index of the internal waveguide mode. As a result, the phase can be adjusted under the condition of the same structure, thickness, and a phase coverage range of $0\sim2\pi$ can be achieved [14].

According to the principle of transmission phase control, the equivalent refractive index of the unit cells can be adjusted by changing the geometry of the nano-dielectric-column, thereby adjusting the phase of the incident light. The optical properties of the designed unit cells are analyzed by the FDTD software. The unit cells are consisted of the SiO_2 substrates and Silicon nano-dielectric-columns. The substrate width of the unit cell is 0.5 μm while the wavelength of the incident light is 1.55 μm. The influence of the nanopillar radius and height on the phase and transmittance is analyzed by simulating a single nanometer dielectric pillar, and the results are shown in Fig.2(a). The phase and transmittance change with the radius for the nanopillar height of 1.3 μm are shown in Fig.2(b). It can be seen that the phase distribution meets the requirements of 0 to π for the SRL and the transmittance is always at a high value exceeding 0.95, with the pillar radii range from 50 nm to 200 nm.

The Fermat Spiral structure with uniform spatial density used in this letter is a bio-inspired structure, with array elements placed on the lattice position imitated sunflower seeds [15]. In previous studies, the Fermat Spiral structure was widely implemented in phased arrays [16]. The results show that the coherent synthesis of the spiral array has lower side-lobe energy and obtains higher energy at the far-field center than the periodic arranged array [17], [18]. Therefore, the automatic aperiodic distribution of the array elements is expected to realize the sidelobe suppression of the super-oscillatory focal field.

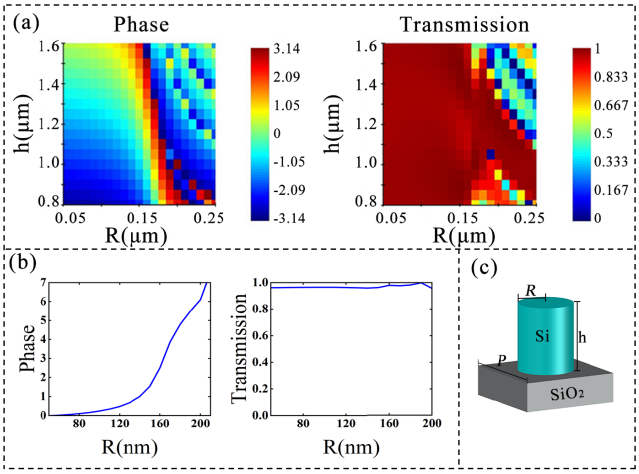

Fig. 2. Unit cell of the bio-inspired Fermat Spiral-arranged SRL. (a) Variation of phase and transmittance with the height(h) and radius of nanopillars. (b) Phase and transmittance varying with the nanopillar radius when the nanopillar height is fixed to be 1.3 μm. (c) Schematic diagram of unit cell structure.

The mathematical expression of the Fermat Spiral is:

$$\rho_n = s\sqrt{\frac{n}{\pi}}$$
$$\phi_n = 2\pi n\beta_1 \tag{2}$$

in the formula, n is an integer with the value range from 1 to $N+1$; $\rho_n$is the distance between the center of the nth unit cell and the center of the spiral; ϕ_n represents the angle of the nth unit cell relative to the position of the polar axis; β_1 controls the two continuous angular displacement between elements; s represents the distance between adjacent array elements on the x-y plane.

In order to realize the focusing function of the SRL, it is necessary to generate a phase distribution that can completely cover 0 to 2π. The phase required by each nanopillar satisfies the following formula:

$$\varphi(x, y) = -\frac{2\pi}{\lambda}(\sqrt{x^2 + y^2 + f^2} - f) \tag{3}$$

where λ is the wavelength of the incident wave; x and y are the horizontal and vertical coordinate of the center of the nanopillars; f is the focal length of the designed SRL.

When simulating a single nanopillar, the radius of the dielectric column varies with a fixed height value, and the relationship between the phase and different radius is obtained at the same time. According to the mathematical expression of Fermat Spiral, the angular displacement and the distance between the two unit cells is 1.618 and 0.5 μm. The position coordinates of each nanopillar are determined by the structure of the Fermat Spiral, and the spatial structure of the SRL is generated according to the relationship between phase and radius. The SRL consists of 767 nanopillars, where the radii of the substrate and lens part are 12 μm and 7.8 μm, respectively, and the radius of a single nanopillar varies according to the position. The generated phase curves are compared with the ideal ones for different focal lengths. When the focal length

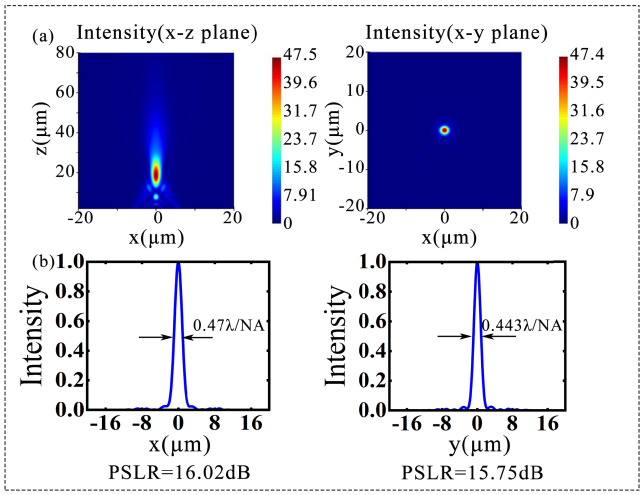

Fig. 3. Focusing performance of the designed SRL at 1550 nm (a) Light field distribution along the propagation direction and at the focal plane. (b) Light field distribution of light field along the x-axis and the y-axis at the focal plane.

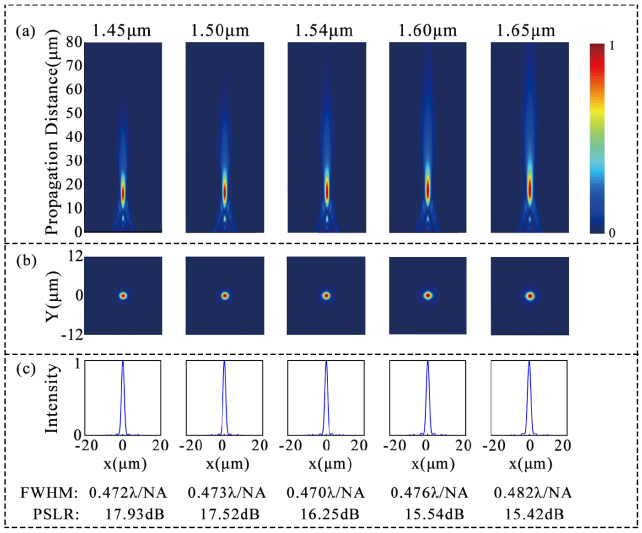

Fig. 4. Focusing performance of the SRL at 1.45 μm, 1.50 μm, 1.54 μm, 1.60 μm and 1.65 μm. (a) Light field distributions along the propagation z direction. (b) Intensity distributions at the focal plane. (c) Light field distribution of light field along the x-axis at the focal plane.

is 22 μm, the generated phase curve is the closest to the idea one, and can cover the phase range required by the SRL.

III. Focusing Properties of the Designed SRL

The focusing properties of the designed SRL are investigated, and the simulation results are shown in Fig.3. A plane wave with a wavelength of 1.55 μm is adopted as the incident illuminating. The NA of the designed SRL is calculated to be 0.386. It is obvious that the sidelobe energy near the focal point of the SRL is very low, indicating that the Fermat Spiral arrangement can effectively suppress the sidelobes, and the PSLR reach 16.02 dB. The full width at half maxima (FWHM) of the focal point along the x-axis and y-axis are about $0.47\frac{\lambda}{NA}$ and $0.443\frac{\lambda}{NA}$, respectively, which are smaller than the Abbe diffraction limit. The ratio of the energy in the area with a diameter of 3 times the FWHM to the total energy of the focal plane is used as the focusing efficiency [19], and the focusing efficiency is calculated to be 72.8%.

In previous studies, SOLs generally only work at a single wavelength, however, the realization of broadband and achromatic is required in many application fields [20], [21], [22], [23], [24]. Subsequently, the achromatic properties of the designed SRL are discussed. Due to the asymmetrical focal spots, the distributions of light field along the x-axis are mainly discussed. The simulation results are shown in Fig.4. It can be seen that the sidelobe energy at the focal point is always at a very low level for different considered wavelengths. The FWHMs of the focal points are $0.472\frac{\lambda}{NA}$, $0.473\frac{\lambda}{NA}$, $0.47\frac{\lambda}{NA}$, $0.476\frac{\lambda}{NA}$, $0.482\frac{\lambda}{NA}$ for the wavelength of 1.45 μm, 1.50 μm, 1.54 μm, 1.60 μm, 1.65 μm, respectively, and the PSLRs are 17.93 dB, 17.52 dB, 16.25 dB, 15.54 dB, 15.42 dB for the five discrete wavelengths.

In order to further demonstrate the achromatic properties of the designed SRL, we investigate the effect of wavelength on the three main properties of the focusing process within the wavelength range from 1.45 μm to 1.65 μm, including the FWHM, the focusing efficiency and the PSLR. The simulation

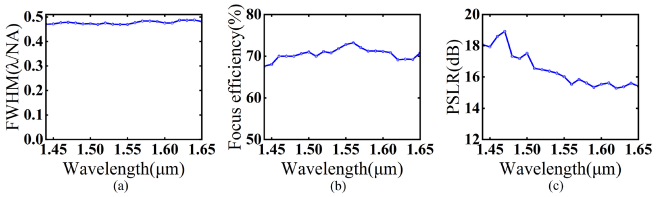

Fig. 5. Achromatic properties of the designed SRL. Simulation tests of (a) FWHM, (b) focusing efficiency, and (c) PSLR as a function of operating wavelength are carried out respectively.

results are shown in Fig. 5, with the working wavelength from 1.45 μm to 1.65 μm. In the whole considered working wavelength range, the FWHMs are all smaller than the Abbe diffraction limit, of which the minimum value is $0.47\frac{\lambda}{NA}$, while the maximum value is $0.488\frac{\lambda}{NA}$, in addition, the FWHM increases with the increase of wavelength. The focusing efficiencies of the designed SRL are higher than 67.8% in the 200 nm-wide wavelength range, and show a trend of increasing and then decreasing. The focusing efficiencies decrease faster when the wavelength less than 1.45 μm, while the focusing efficiencies gradually decrease for the wavelength larger than 1.55 μm. The largest focusing efficiency exhibits at 1.55 μm, because the generated lens phased is designed closed to the ideal lens phase at 1.55 μm. In particular, the PSLRs maintain a high level better than 15.29 dB in the 200 nm wide band, and the PSLRs show an overall decreasing trend with the increase of wavelength. The sidelobe suppression benefits from the aperiodic distribution of Fermat Spiral-arranged unit cells, and do not depend on the generated phase distribution. Therefore, the working bandwidth of the proposed bio-inspired SRL can reach at least 200 nm with the superiority of the three main properties of the focusing.

The proposed SRL has high aspect ratio, fabrication processing can use deep-ultraviolet (DUV) projection stepper lithography [25]. The phase manipulation of the designed SRL

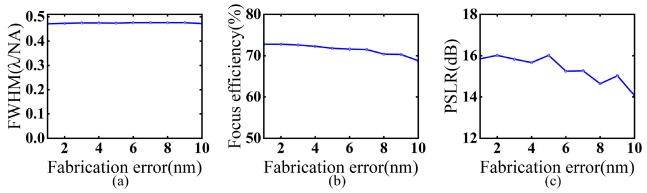

Fig. 6. Fabrication error tolerance of the designed SRL. Simulation results of (a) FWHM, (b) focusing efficiency and (c) PSLR with the fabrication errors of 1-10 nm.

is achieved by precisely adjusting the radius of the nanopillar, and the deviation of the nanopillars radii from the ideal value caused by fabrication processing has a non-negligible impact on the focusing effect. It's necessary to analyze the fabrication tolerance of the designed SRL. On the basis of the designed SRL, the radii of the nanopillars are randomly added with an error. We investigate the effect of fabrication error on the three main properties of the focusing process, including the FWHM, the focusing efficiency and the PSLR. As shown in Fig.6, it can be seen that the FWHMs show irregular changes with fabrication errors of 1-10 nm, and all of them are smaller than the diffraction limit. The focusing efficiency gradually decreases with fabrication error increasing, when the processing error exceeds 9nm, the focusing efficiency is lower than 70%, and the decline becomes fast. The PSLRs also decrease with the error increasing, but all of them are at a high level exceeding 14.07 dB, and the influence on the far-field center spot is small. Therefore, the SRL has a high focusing efficiency as well as PSLR, even within the fabrication error as large as 9 nm, so the designed SRL has the advantage of large fabrication error tolerance, which provides a new method to reduce the required fabrication accuracy of the SRL.

IV. Conclusion

In this letter, a bio-inspired Fermat Spiral SRL with uniform spatial density distribution has been designed. The results show that the Fermat Spiral structure can effectively suppress the sidelobe energy with the PSLR of 16.02 dB at 1550 nm and the FWHM is $0.47\frac{\lambda}{NA}$. A wide working bandwidth of 200 nm are achieved, with the focusing efficiencies and PSLRs higher than 67.8% and 15.29 dB, respectively. In addition, the designed SRL exhibits a large fabrication error tolerance of 9 nm. The low-sidelobe and achromatic SRL provides a promising approach for the micro-imaging, data storage, holography, etc.

References

[1] F. Ali and S. Aksu, "A hybrid broadband metalens operating at ultraviolet frequencies," *Sci. Rep.*, vol. 11, no. 1, p. 2303, Jan. 2021, doi: 10.1038/s41598-021-81956-4.

[2] Y. Wang et al., "High-efficiency broadband achromatic metalens for near-IR biological imaging window," *Nature Commun.*, vol. 12, no. 1, p. 5560, Sep. 2021, doi: 10.1038/s41467-021-25797-9.

[3] M. Han, W. Fu, D. Lu, C. Zhang, Y. Li, and Y. Yan, "All-dielectric metalens for quasi-optical mode and polarization conversion," *Opt. Exp.*, vol. 30, no. 19, pp. 34797–34808, 2022.

[4] Y. Mohtashami et al., "Light-emitting metalenses and meta-axicons for focusing and beaming of spontaneous emission," *Nature Commun.*, vol. 12, no. 1, p. 3591, Jun. 2021, doi: 10.1038/s41467-021-23433-0.

[5] F. M. Huang and N. I. Zheludev, "Super-resolution without evanescent waves," *Nano Lett.*, vol. 9, no. 3, pp. 1249–1254, Mar. 2009.

[6] K. Huang, H. Ye, J. Teng, S. P. Yeo, B. Luk'yanchuk, and C.-W. Qiu, "Optimization-free superoscillatory lens using phase and amplitude masks," *Laser Photon. Rev.*, vol. 8, no. 1, pp. 152–157, Jan. 2014, doi: 10.1002/lpor.201300123.

[7] P. He, W. Li, C. An, X. Sun, W. Yuan, and Y. Yu, "Sub-diffraction-limit light sheet enabled by a super-oscillatory lens with an enlarged field of view and depth of focus," *Opt. Lett.*, vol. 47, no. 13, p. 3267, 2022, doi: 10.1364/ol.461730.

[8] M. Khorasaninejad et al., "Polarization-insensitive metalenses at visible wavelengths," *Nano Lett.*, vol. 16, no. 11, pp. 7229–7234, Nov. 2016, doi: 10.1021/acs.nanolett.6b03626.

[9] X. Lu et al., "Switchable polarization-multiplexed super-oscillatory metasurfaces for achromatic sub-diffraction focusing," *Opt. Exp.*, vol. 28, no. 26, p. 39024, 2020, doi: 10.1364/oe.413078.

[10] Z. X. Wu et al., "Binary-amplitude modulation based super-oscillatory focusing planar lens for azimuthally polarized wave," *Opto-Electron. Eng.*, vol. 45, no. 4, pp. 68–76, 2018.

[11] Q. Lou and Z. N. Chen, "Sidelobe suppression of metalens antenna by amplitude and phase controllable metasurfaces," *IEEE Trans. Antennas Propag.*, vol. 69, no. 10, pp. 6977–6981, Oct. 2021, doi: 10.1109/TAP.2021.3076312.

[12] Q. Lou and Z. N. Chen, "Flat-focal-plane dual-metasurface lens for low scan loss and sidelobe level of a metalens antenna," *IEEE Trans. Antennas Propag.*, vol. 70, no. 10, pp. 9849–9854, Oct. 2022.

[13] L.-X. Wu et al., "Transmissive metasurface with independent amplitude/phase control and its application to low-side-lobe metalens antenna," *IEEE Trans. Antennas Propag.*, vol. 70, no. 8, pp. 6526–6536, Aug. 2022.

[14] S. M. Kamali, E. Arbabi, A. Arbabi, and A. Faraon, "A review of dielectric optical metasurfaces for wavefront control," *Nanophotonics*, vol. 7, no. 6, pp. 1041–1068, Jun. 2018, doi: 10.1515/nanoph-2017-0129.

[15] M. C. Viganó, G. Toso, G. Caille, C. Mangenot, and I. E. Lager, "Sunflower array antenna with adjustable density taper," *Int. J. Antennas Propag.*, vol. 2009, pp. 1–10, Jan. 2009, doi: 10.1155/2009/624035.

[16] G. Allevato et al., "Air-coupled ultrasonic spiral phased array for high-precision beamforming and imaging," *IEEE Open J. Ultrason., Ferroelectr., Freq. Control*, vol. 2, pp. 40–54, 2022.

[17] K. Encino, M. A. Panduro, A. Reyna, and D. H. Covarrubias, "Novel design techniques for the Fermat spiral in antenna arrays, for maximum SLL reduction," *Micromachines*, vol. 13, no. 11, p. 2000, Nov. 2022.

[18] Y. Gao, J. Liao, J. Xu, and Z. Zhou, "Sidelobe suppression for coherent beam combining with laser beams placed along a Fermat spiral," *Chin. Opt. Lett.*, vol. 20, no. 2, 2022, Art. no. 021405.

[19] Y. Zheng et al., "Designing high-efficiency extended depth-of-focus metalens via topology-shape optimization," *Nanophotonics*, vol. 11, no. 12, pp. 2967–2975, May 2022, doi: 10.1515/nanoph-2022-0183.

[20] X. Lu et al., "Broadband achromatic metasurfaces for sub-diffraction focusing in the visible," *Opt. Exp.*, vol. 29, no. 4, pp. 5947–5958, 2021, doi: 10.1364/OE.417036.

[21] L. Chen, J. Liu, X. Zhang, and D. Tang, "Achromatic super-oscillatory metasurface through optimized multiwavelength functions for sub-diffraction focusing," *Opt. Lett.*, vol. 45, no. 20, pp. 5772–5775, 2020, doi: 10.1364/OL.404764.

[22] Y. Zhang et al., "Band-tunable achromatic metalens based on phase change material," *Opt. Exp.*, vol. 30, no. 10, pp. 17541–17553, 2022.

[23] D. Shan et al., "Design of the all-silicon long-wavelength infrared achromatic metalens based on deep silicon etching," *Opt. Exp.*, vol. 30, no. 8, pp. 13616–13629, 2022.

[24] Y. Zheng et al., "Broadband achromatic metalens in the long-wave infrared regime," *IEEE Photon. J.*, vol. 15, no. 2, pp. 1–7, Apr. 2023, doi: 10.1109/JPHOT.2023.3243409.

[25] J.-S. Park et al., "All-glass, large metalens at visible wavelength using deep-ultraviolet projection lithography," *Nano Lett.*, vol. 19, no. 12, pp. 8673–8682, Dec. 2019, doi: 10.1021/acs.nanolett.9b03333.